PHYSICAL REVIEW C **76**, 034309 (2007)

# Low densities in asymmetric nuclear matter

Jérôme Margueron
*Institut de Physique Nucléaire, Université Paris-Sud, $IN_2P_3$-CNRS, F-91406 Orsay Cedex, France*

Eric van Dalen
*Departament d'Estructura i Constituents de la Matèria, Universitat de Barcelona, Diagonal 647, E-08028 Barcelona, Spain*

Christian Fuchs
*Institut für Theoretische Physik, Universität Tübingen, D-72076 Tübingen, Germany*
(Received 28 June 2007; published 7 September 2007)

Asymmetric nuclear matter is investigated in the low-density region below the nuclear saturation density. Microscopic calculations based on the Dirac-Brueckner-Hartree-Fock (DBHF) approach with realistic nucleon-nucleon potentials are used to adjust a low-density functional. This functional is constructed on a density expansion of the relativistic mean-field theory that allows a clear interpretation of the role of the mesons in the equation of state. It is shown that a correction term should be added to the functional to take into account the effects beyond the mean field. Two functionals with different corrections are obtained and their topological properties have been studied. Those functionals converge to predict a reduction of the spinodal zone in asymmetric nuclear matter by about 15–20% and an isoscalar unstable mode closer to the constant $Z/A$ direction than the functional without correction.

DOI: 10.1103/PhysRevC.76.034309 PACS number(s): 25.70.Pq, 21.65.+f, 24.10.Pa, 26.60.+c

## I. INTRODUCTION

How do nuclear matter properties change when the density decreases from saturation densities? In this low-density regime, what is the role of isospin asymmetry? Indeed, although the nuclear density functional below saturation density has not been studied much it has importance for several topics concerning atomic nuclei surface properties, the equation of state of the core of neutron stars, and the dynamical description of heavy-ion collisions, both at intermediate and relativistic energies. Recently, several attempts have been made to establish a relation between the low-density equation of state and nuclear properties such as surface behavior and pairing properties [1–4], neutron radii [5], or the spinodal instability [6]. Those works are based on phenomenological density functionals or fits of ab initio calculations but without considering the very low properties of the equation of state. Below saturation density, the effects of two-body correlations are important and induce anomalies in the density dependence of the equation of state [7].

Models that make predictions for the nuclear equation of state (EOS) can roughly be divided into three classes: phenomenological density functionals, effective field theory approaches, and ab initio approaches. The phenomenological density functionals are based on effective density-dependent interactions such as Gogny or Skyrme forces [8,9] or relativistic mean-field (RMF) models [10]. Parameters are adjusted to nuclear bulk properties and finite nuclei. Effective field theory (EFT) approaches are based on a perturbative expansion of the nucleon-nucleon interaction or the nuclear mean field within power-counting schemes. These approaches lead to a more systematic expansion of the EOS in powers of density, respectively, the Fermi momentum $k_F$. The EFT approaches can be based on density functional theory [11,12] or, for example, on chiral perturbation theory [13,14]. The advantage of EFT is the small number of free parameters and a correspondingly higher predictive power. However, when high-precision fits are intended, the EFT functionals are based on approximately the same number of model parameters as phenomenological density functionals because of fine-tuning through additional parameters.

Ab initio approaches are based on high-precision free-space nucleon-nucleon interactions. In addition, predictions for the nuclear EOS are parameter free. Examples of such approaches are variational calculations [15,16], Brueckner-Hartree-Fock (BHF) [17–20] or relativistic Dirac-Brueckner-Hartree-Fock (DBHF) [21–26] calculations, and Green's function Monte Carlo approaches (GFMC) [27–29]. Nonrelativistic ab initio calculations do not meet the empirical region of saturation, whereas relativistic calculations do a better job. This deficiency can be solved by the explicit inclusion of three-body forces where the relativistic approach accounts already effectively for part of these contributions. For a more detailed discussion see, for example, Ref. [20].

In the present work microscopic calculations based on the DBHF approach [26] using a realistic nucleon-nucleon potential (i.e., the Bonn A interaction [30]) are used to obtain a functional that describes the EOS from low densities up to saturation density. The construction of this functional is motivated by RMF theory [31,32]. Since both DBHF and RMF are relativistic approaches based on Dirac phenomenology they have similar features, in particular the occurrence of large and canceling scalar and vector fields in the isoscalar sector. That the occurrence of such fields is a fundamental consequence of the elementary nuclear force has recently been shown in Ref. [33]. Similar fields, which are, however, smaller, also occur in the isovector sector. Thus, RMF theory is well suited for the present investigations. However, RMF theory is

 

insufficient to reproduce the more complex nonlinear behavior of the DBHF energy density near $\rho_B = 0.1$ fm$^{-3}$, where for instance effects of the deuteron pole show up. Corrections beyond the mean field are necessary and the nonlinear behavior is then corrected by adding new terms to the functional.

The paper is organized as follows: The relativistic DBHF is shortly sketched in Sec. II. Section III is devoted to the relativistic mean-field approach and the series expansion in the baryonic density. This expansion allows a clear interpretation of the meson contributions to the equation of state. The parameters of the functionals are obtained in Sec. IV. With these density functionals the dynamics of the liquid-gas transition induced by heavy-ion collisions at Fermi energies (i.e., the spinodal instabilities) are investigated and analyzed in Sec. V. Finally, we end with a conclusion in Sec. VI.

## II. DBHF APPROACH

We consider homogeneous nuclear matter at low density so that two-body correlations dominate. Of course, at very low density, clustering phenomena can occur (e.g., deuteron, tritium, helium, and $\alpha$-particle formation) [7,34,35]. Therefore, we are going to consider densities that are low with respect to saturation density but still large compared to typical values where the onset of clustering occurs. Typically, we are considering densities between about one-tenth to one-half of the saturation density. In this density region, microscopic calculations based on the relativistic DBHF approach [21,24–26,36] are expected to be quite accurate, and they will be, therefore, the starting point of our analysis.

In the relativistic Brueckner approach the nucleon inside the medium is dressed by the self-energy $\Sigma$. The in-medium $T$ matrix, which is obtained from the relativistic Bethe-Salpeter (BS) equation, plays the role of an effective two-body interaction that contains all short-range and many-body correlations of the ladder approximation. In solving the BS equation the Pauli principle is respected and intermediate scattering states are projected out of the Fermi sea. The summation of the $T$ matrix over the occupied states inside the Fermi sea yields finally the self-energy in the Hartree-Fock approximation. This coupled set of equations states a self-consistency problem that has to be solved by iteration. Technical details of the present DBHF calculations, in particular the treatment of isospin asymmetry, can be found in Ref. [26]. The results are based on the Bonn A one-boson-exchange potential for the bare nucleon-nucleon interaction [30].

Figure 1 compares the prediction for the low-density regime of symmetric nuclear matter (below zero) and pure neutron matter (above zero) from microscopic many-body approaches. It shows in addition the equations of state obtained by two typical phenomenological RMF models. From the microscopic side these are the DBHF results [26], which will be further analyzed, nonrelativistic Brueckner (BHF) calculations from Ref. [1], and variational calculations from Ref. [16]. The variational and BHF calculations are based on the $AV_{18}$ Argonne potential. The variational calculations include in addition phenomenological three-body forces

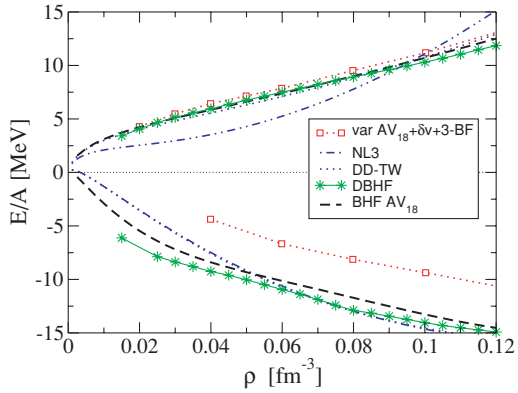


FIG. 1. (Color online) Comparison of several equations of state with the DBHF results. The DBHF calculations are represented by the stars, the variational calculations by the empty squares, the nonrelativistic Brueckner results by the dashed line, and two different relativistic mean-field parametrizations NL3 and DD-TW by dashed-dotted and dotted lines, respectively.

(Urbana IX) and relativistic boost corrections, neither of which, however, play an important role in the low-density regime. The phenomenological models are the well-established NL3 [37] RMF parametrization and the RMF model of Ref. [38] (DD-TW). The latter is a phenomenological version of density-dependent RMF theory using density-dependent meson-nucleon couplings [39], which allows for a larger freedom in the adjustment of the EOS. Both approaches fit finite-nuclei properties with high accuracy.

The first thing that becomes evident from Fig. 1 is the remarkable agreement of the microscopic approaches (DBHF, BHF, and variational) for the pure neutron matter EOS. This agreement indicates that both the interaction and the many-body schemes are well controlled in the $nn$ sector at low densities. This is because of the large $nn$ scattering length and the lack of clustering phenomena ($d, \alpha$, etc.), which make the treatment of neutron matter at subnuclear densities less model dependent. In this context it is worth noticing that the microscopic calculations (BHF, DBHF, and variational) are consistent with the low-density limit of "exact" quantum–Monte Carlo calculations for neutron matter [27] and with the result of the renormalization group $V_{\mathrm{lowk}}$ approach [40].

The situation seems to be different for symmetric nuclear matter. The Brueckner calculations show significantly more binding than the variational calculations of Ref. [16]. However, the DBHF and BHF results are very close and exhibit the same low-density behavior: In contrast to RMF theory and also to the results of Ref. [16] one can observe a nonlinear convergence to zero when the density decreases. This fact is associated with the deuteron channel and can possibly be interpreted as a manifestation of the onset of the superfluid phase. In this context it is interesting to note that a recent study of low-density nuclear matter [7], based on a virial expansion that includes protons, neutrons and $\alpha$-particle degrees of freedom, revealed a low-density EOS taht is in qualitative agreement with the DBHF predictions. In the virial approach the binding energy goes smoothly to zero for neutron matter

while the energy per particle $E/A$ minus the (free) kinetic energy in symmetric matter remains practically constant at a value of around $-8$ MeV down to extremely low densities ($\rho_B \simeq 0.0002$ fm$^{-3}$) before it rapidly drops to zero (Fig. 15 in Ref. [7]). Subtracting the kinetic energy of a nonrelativistic Fermi gas, $3k_F^2/10M$, from the DBHF result yields at $k_F = 0.5$ fm$^{-1}$ ($\rho_B = 0.0084$ fm$^{-3}$) a value of $-8.4$ MeV, which coincides remarkably well with the virial low-density limit.

## III. SERIES EXPANSION OF THE RMF LAGRANGIAN IN THE BARYONIC DENSITY

A Lagrangian density of an interacting many-particle system consisting of nucleons, isoscalar (scalar $\sigma$, vector $\omega$), and isovector (scalar $\delta$, vector $\rho$) mesons is the starting point of the RMF theory:

$$\begin{aligned}\mathcal{L} = \bar{\psi}[i\gamma_\mu\partial^\mu - (M - g_\sigma\sigma - g_\delta\vec{\tau}\cdot\vec{\delta}) \\ - g_\omega\gamma_\mu\omega^\mu - g_\rho\gamma^\mu\vec{\tau}\cdot\vec{\rho}_\mu]\psi + \tfrac{1}{2}\left(\partial_\mu\sigma\partial^\mu\sigma - m_\sigma^2\sigma^2\right) \\ - U(\sigma) + \tfrac{1}{2}m_\omega^2\omega_\mu\omega^\mu + \tfrac{1}{2}m_\rho^2\vec{\rho}_\mu\cdot\vec{\rho}^\mu \\ + \tfrac{1}{2}\left(\partial_\mu\vec{\delta}\cdot\partial^\mu\vec{\delta} - m_\delta^2\vec{\delta}^2\right) - \tfrac{1}{4}F_{\mu\nu}F^{\mu\nu} - \tfrac{1}{4}\vec{G}_{\mu\nu}\vec{G}^{\mu\nu}, \quad (1)\end{aligned}$$

where $\sigma$ is the $\sigma$-meson field, $\omega_\mu$ is the $\omega$-meson field, $\vec{\rho}_\mu$ is $\rho$-meson field, and $\vec{\delta}$ is the isovector scalar field of the $\delta$ meson, and where $F_{\mu\nu} \equiv \partial_\mu\omega_\nu - \partial_\nu\omega_\mu$, $\vec{G}_{\mu\nu} \equiv \partial_\mu\vec{\rho}_\nu - \partial_\nu\vec{\rho}_\mu$, and the $U(\sigma)$ is a nonlinear potential of $\sigma$ meson: $U(\sigma) = \frac{1}{3}a\sigma^3 + \frac{1}{4}b\sigma^4$. Dynamical equations deduced at the mean-field approximation are presented in Appendix A. We refer to the appendix for all the standard definitions. Hereafter, we introduce the coupling constants $f_i = g_\rho/m_i$ for $i = \sigma, \delta, \omega$, and $\rho$, and the nonlinear constant $f_\sigma^{\rm nl} = a(f_\sigma/m_\sigma)^3$. In the following the energy density $\epsilon$ is expanded up to a power of 4 in proton and neutron densities. The expression for the density of energy is given in Appendix A. For the linear version of the RMF model, that is, without a nonlinear $\sigma$-meson potential $U(\sigma)$, such an expansion can be found in Ref. [41]. Here we extend this expansion to the nonlinear case and to the isospin sector, that is, to $\rho_p \neq \rho_n$ (i.e., the isovector mesons $\rho$ and $\delta$ are included). Notice, however, that in the present form only the nonlinear term with the coupling constant $a$ is included because the one with the coupling constant $b$ contributes to higher terms in the density expansion.

The scalar field is the solution of the following self-consistent equation:

$$g_\sigma\sigma = f_\sigma^2\rho_s - \frac{a}{g_\sigma m_\sigma^2}(g_\sigma\sigma)^2 - \frac{b}{(m_\sigma g_\sigma)^2}(g_\sigma\sigma)^3. \quad (2)$$

A low-density approximate solution is presented in Appendix B. The solution is expressed as a function of the scalar density $\rho_s$,

$$g_\sigma\sigma = f_\sigma^2\rho_s - f_\sigma^{\rm nl}\rho_s^2 + o\left(\rho_{si}^3\right). \quad (3)$$

The low-density expansion of the scalar density $\rho_{si}$ is then required. It yields

$$\begin{aligned}\rho_{si} = \rho_i - \frac{3}{10M_i^{*2}}\left(\frac{6\pi^2}{\gamma}\right)^{2/3}\rho_i^{5/3} \\ + \frac{9}{56M_i^{*4}}\left(\frac{6\pi^2}{\gamma}\right)^{4/3}\rho_i^{7/3}\frac{15}{144M_i^{*6}}\left(\frac{6\pi^2}{\gamma}\right)^2\rho_i^3 \\ + \frac{105}{1408M_i^{*8}}\left(\frac{6\pi^2}{\gamma}\right)^{8/3}\rho_i^{11/3} + o\left(\rho_i^4\right), \quad (4)\end{aligned}$$

where $\gamma$ is the degeneracy of the system. Note that this expansion is also a relativistic expansion in the parameter $k_{Fi}/M_i^*$.

Neutron and proton Dirac masses, also called the scalar masses, are expressed in terms of the scalar and isoscalar fields. By using Eq. (3) and Eq. (5), the low-density expansion of the Dirac masses is given by ($-$ proton, $+$ neutron)

$$\begin{aligned}M_i^* = M - f_\sigma^2\Big[\rho_B - \frac{3}{10M^2}(3\pi^2)^{2/3}\left(\rho_p^{5/3} + \rho_n^{5/3}\right) \\ + \frac{9}{56M^4}(3\pi^2)^{4/3}\left(\rho_p^{7/3} + \rho_n^{7/3}\right) - \frac{3}{5M^3}f_\sigma^2(3\pi^2)^{2/3} \\ \times\left(\rho_p^{8/3} + \rho_n^{8/3}\right)\Big] \pm f_\delta^2\Big[\rho_3 - \frac{3}{10M^2}(3\pi^2)^{2/3} \\ \times\left(\rho_p^{5/3} - \rho_n^{5/3}\right) + \frac{9}{56M^4}(3\pi^2)^{4/3}\left(\rho_p^{7/3} - \rho_n^{7/3}\right) \\ - \frac{3}{5M^3}f_\delta^2(3\pi^2)^{2/3}\left(\rho_p^{8/3} - \rho_n^{8/3}\right)\Big] \\ + f_\sigma^{\rm nl}\left[\rho_B^2 - \frac{3}{5M^2}(3\pi^2)^{2/3}\rho_B\left(\rho_p^{5/3} + \rho_n^{5/3}\right)\right] + o\left(\rho_i^3\right). \quad (5)\end{aligned}$$

Now, we evaluate the full density functional,

$$\begin{aligned}\epsilon = \epsilon_{\rm kin} + \tfrac{1}{2}f_\sigma^2\rho_s^2 - \tfrac{2}{3}f_\sigma^{\rm nl}\rho_s^2 + \tfrac{1}{2}f_\omega^2\rho_B^2 \\ + \tfrac{1}{2}f_\rho^2\rho_3^2 + \tfrac{1}{2}f_\delta^2\rho_{s3}^2 + o(\rho^4), \quad (6)\end{aligned}$$

where $\epsilon_{\rm kin}$ is the kinetic term. The density functional is decomposed into several terms:

$$\begin{aligned}\epsilon(\rho_n, \rho_p) = M\rho_B + \epsilon_{\rm FG}(\rho_n, \rho_p) + \epsilon_L(\rho_n, \rho_p) \\ + \epsilon_{\rm NL}(\rho_n, \rho_p) + o(\rho^4), \quad (7)\end{aligned}$$

where the term $\epsilon_{\rm FG}$ is the contribution of the free Fermi gas without the rest mass, the term $\epsilon_L$ is generated by the interactions and the Dirac mass, and the term $\epsilon_{\rm NL}$ is the correction coming from the nonlinear $\sigma$ coupling. In the following, we give explicitly the form of those terms, classified according to the power in Fermi momentum (=power in density divided by 3) to have an integer index. The pure kinetic contributions (FG) are $\epsilon_{\rm FG} = \epsilon_{\rm FG,5} + \epsilon_{\rm FG,7} + \epsilon_{\rm FG,9} + \epsilon_{\rm FG,11}$

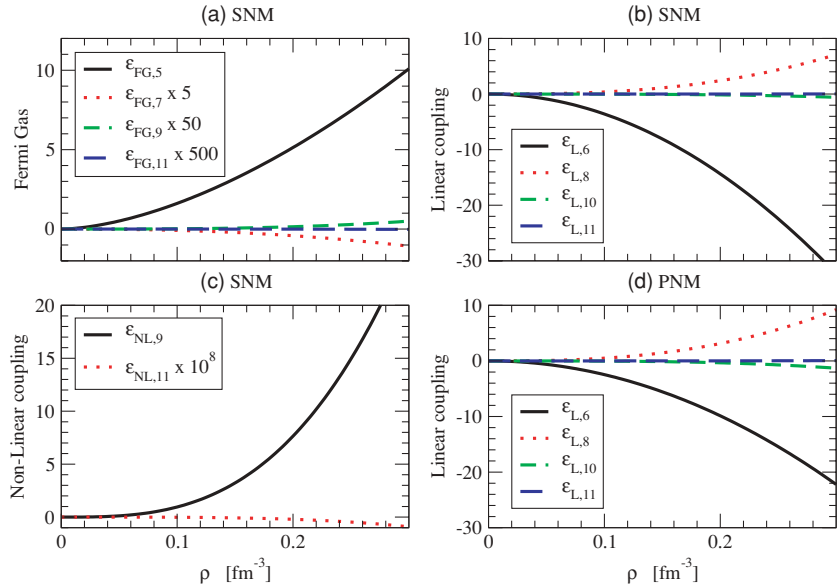


FIG. 2. (Color online) Representation of the different terms in the series expansion of the energy functional with respect to the baryonic density, up to 0.3 fm$^{-3}$. The first three subsets show the fast convergence in symmetric nuclear matter (SNM) and the last subset (d) shows the contribution of the isovector mesons in pure neutron matter (PNM). To give an idea of the fast convergence, we have multiplied some of the terms by huge constants. The coupling constants (set A NL$\rho\delta$) obtained by Liu *et al.* [42] have been used.

up to a power of 4 in the densities, where

$$\epsilon_{\mathrm{FG},5}(\rho_n,\rho_p)=\frac{3}{10M}(3\pi^2)^{2/3}\left(\rho_p^{5/3}+\rho_n^{5/3}\right), \tag{8}$$

$$\epsilon_{\mathrm{FG},7}(\rho_n,\rho_p)=-\frac{3}{56M^3}(3\pi^2)^{4/3}\left(\rho_p^{7/3}+\rho_n^{7/3}\right), \tag{9}$$

$$\epsilon_{\mathrm{FG},9}(\rho_n,\rho_p)=\frac{1}{48M^5}(3\pi^2)^{2}\left(\rho_p^{3}+\rho_n^{3}\right), \tag{10}$$

$$\epsilon_{\mathrm{FG},11}(\rho_n,\rho_p)=-\frac{15}{1408M^7}(3\pi^2)^{8/3}\left(\rho_p^{11/3}+\rho_n^{11/3}\right). \tag{11}$$

The contribution of the mesons (with only linear couplings) and Dirac mass contribution is $\epsilon_L=\epsilon_{L,6}+\epsilon_{L,8}+\epsilon_{L,10}+\epsilon_{L,11}$, where

$$\epsilon_{L,6}(\rho_n,\rho_p)=\frac{1}{2}\left(-f_\sigma^2+f_\omega^2\right)\rho_B^2+\frac{1}{2}\left(-f_\delta^2+f_\rho^2\right)\rho_3^2, \tag{12}$$

$$\epsilon_{L,8}(\rho_n,\rho_p)=\frac{3}{10M^2}(3\pi^2)^{2/3}\left[f_\sigma^2\rho_B\left(\rho_p^{5/3}+\rho_n^{5/3}\right)+f_\delta^2\rho_3\left(\rho_p^{5/3}-\rho_n^{5/3}\right)\right], \tag{13}$$

$$\begin{aligned}\epsilon_{L,10}(\rho_n,\rho_p)=&-\frac{9}{M^4}\left(3\pi^2\right)^{4/3}f_\sigma^2\left[\frac{1}{56}\left(\rho_p^{7/3}+\rho_n^{7/3}\right)\rho_B+\frac{1}{200}\left(\rho_p^{5/3}+\rho_n^{5/3}\right)^2\right]\\&-\frac{9}{M^4}(3\pi^2)^{4/3}f_\delta^2\left[\frac{1}{56}\left(\rho_p^{7/3}-\rho_n^{7/3}\right)\rho_3+\frac{1}{200}\left(\rho_p^{5/3}-\rho_n^{5/3}\right)^2\right],\end{aligned} \tag{14}$$

$$\begin{aligned}\epsilon_{L,11}(\rho_n,\rho_p)=&\frac{3}{10M^3}(3\pi^2)^{2/3}\left[f_\sigma^4\rho_B^2\left(\rho_p^{5/3}+\rho_n^{5/3}\right)\right.\\&+f_\delta^4\rho_3^2\left(\rho_p^{5/3}-\rho_n^{5/3}\right)\\&\left.+2f_\sigma^2f_\delta^2\left(\rho_p^2-\rho_n^2\right)\left(\rho_p^{5/3}-\rho_n^{5/3}\right)\right].\end{aligned} \tag{15}$$

Finally, the first-order corrections induced by the nonlinear $\sigma$ coupling is $\epsilon_{\mathrm{NL}}=\epsilon_{\mathrm{NL},9}+\epsilon_{L,11}$, where

$$\epsilon_{\mathrm{NL},9}(\rho_n,\rho_p)=\frac{1}{3}f_\sigma^{\mathrm{nl}}\rho_B^3, \tag{16}$$

$$\epsilon_{\mathrm{NL},11}(\rho_n,\rho_p)=-\frac{3}{10M^2}f_\sigma^{\mathrm{nl}}(3\pi^2)^{2/3}\rho_B^2\left(\rho_p^{5/3}+\rho_n^{5/3}\right). \tag{17}$$

The convergence of this series expansion is checked in symmetric nuclear matter (SNM) and pure neutron matter (PNM) by using the set of coupling constants, set A NL$\rho\delta$, obtained by Liu *et al.* [42]. We choose this set of parameters because it has been obtained with the same degrees of freedom as those we consider in our Lagrangian. We show in Fig. 2 the contribution of the different terms of the functional up to a power of 4 in the densities. Some terms have been multiplied by a huge factor to distinguish them from each others. The convergence is essentially due to the truncation of powers of $k_F/M$ that comes with our expansion. This figure shows how negligible the terms with large power counting are in the density expansion, even for the higher densities represented (about 0.3 fm$^{-3}$).

In the following the low-density RMF functional defined in Eqs. (7)–(17) will be used to fit the result of the DBHF calculation [26] and to calculate the spinodal instabilities in low-density asymmetric nuclear matter.

## IV. DETERMINATION OF THE PARAMETERS OF THE FUNCTIONAL

In this section, we fit the result of the DBHF calculation (Dirac mass, energy density, and binding energies) in the density region between 0.01 and 0.2 fm$^{-3}$ using the low-density RMF functional defined in Eqs. (7)–(17). The fits are based on the density expansion of the RMF Lagrangian (1), which contains nonlinear terms in the scalar $\sigma$ field and linear terms in the vector field $\omega$ as well as in the

isovector $\rho$ and $\delta$ fields. An alternative would be to perform such a parametrization of the DBHF results in terms of density-dependent relativistic hadron (DDRH) theory [38,39,43–45] where nonlinearities from higher order density corrections are absorbed into density-dependent meson-nucleon vertices at the level of the effective Lagrangian. The reason why we have chosen the standard RMF Lagrangian (1) is twofold: First, it allows a well-defined low-density expansion whereas the density dependence of effective meson-nucleon vertices in DDRH theory depends on the choice of a particular ansatz for these functionals. Second, the extraction of such coupling functions from the present DBHF self-energies [26] shows that the DBHF vector self-energy, except for the very low density regime, has a linear density dependence that can be expressed by a linear $\omega$-meson field. Nonlinearities in the scalar channel are absorbed in the nonlinear $\sigma$ terms. The isovector dependence can also be reasonably well fitted through the two isovector $\rho$ and $\delta$ mesons. In summary, such a procedure allows a well-defined comparison of the microscopic DBHF model to RMF phenomenology and a controlled investigation of the low-density regime, where the RMF fits break down and require additional correction terms, as will be seen in the following.

The adjusting procedure is twofold: First, we fit the parameters of the RMF Lagrangian using the relativistic Dirac mass and the energy density in symmetric and asymmetric nuclear matter obtained from the DBHF calculation. The fit includes 23 calculated points between $\rho_B = 0.02$ and 0.13 fm$^{-3}$, plus two densities, $\rho_B = 0.1658$ fm$^{-3}$ and $\rho_B = 0.197$ fm$^{-3}$, for $y = \rho_p/\rho_B = 0$ to 0.5 with a step $= 0.05$. We obtain the set of parameters called RMF presented in Table I, by fitting the Dirac mass and the density of energy and imposing that the functional passes exactly through the point at $\rho_B = 0.197$ fm$^{-3}$ in symmetric nuclear matter and pure neutron matter. The latter condition is imposed to get a value of the symmetry energy close to DBHF, as shown in Table II. Then, we extract and fit the residual difference between the DBHF calculation and the energy per particle in symmetric nuclear matter and pure neutron matter separately. To check the sensitivity of the results on the functional correction, we have investigated two different functionals. In the following, we give the details of the adjusting procedure.

### A. Determination of the $\sigma$ and $\delta$ coupling constants

The low-density expansion of the Dirac mass, Eq. (5), is used to determine the linear sigma coupling constant $f_\sigma$, the scalar isovector $\delta$ meson $f_\delta$, and the nonlinear sigma coupling constant $f_\sigma^{\rm nl}$. We deduce the value of the parameters for the adjustment to DBHF results in asymmetric nuclear matter with $y = \rho_p/\rho_B = 0.5$, 0.3, and 0.0. In Fig. 3 we compare the DBHF results with the best fit. The linear contribution comes from the term $f_\sigma^2\rho_B$ in Eq. (5), then comes the quadratic term $f_\sigma^{\rm nl}\rho_B^2$, and the isospin asymmetry is essentially coming from the first term $f_\delta^2\rho_3$; the contributions of the other terms are negligible. The parameters are given in Table I and are compared to the set A NL$\rho\delta$ proposed in Ref. [42]. The parameters $f_\sigma$ and $f_\delta$ are very similar for the two sets of parameters whereas the parameters $f_\sigma^{\rm nl}$ differ by a factor of 3. In our fit, $f_\sigma^{\rm nl}$ is obtained from the quadratic density dependence of the scalar mass, whereas in the set A NL$\rho\delta$, the nonlinear $\sigma$ coupling is adjusted to reduce the compressibility modulus. As a consequence, we obtain a lower value for the parameter $f_\sigma^{\rm nl}$, and the compressibility modulus is larger than expected. Moreover, to obtain a good fit of the binding energy, the nonlinear term $\epsilon_{\rm NL,9}$ defined in Eq. (16) has to be divided by 2. This may indicate that higher order nonlinearities in the $\sigma$ field and probably also nonlinear $\omega$ terms should be taken into account to obtain a proper description of the DBHF EOS beyond saturation density. However, to keep the formalism as simple as possible we stick to the strandard NL model and apply this phenomenological correction. The saturation properties are shown in Table II. This indicate that one cannot reproduce the scalar mass density dependence and the saturation density with a standard $\sigma$-nonlinear RMF Lagrangian. This illustrates the convenience of using a density functional where the effects of the meson couplings are tractable. In our Lagrangian, the compressibility modulus will be lowered by the correction terms induced by the physics beyond the mean field.

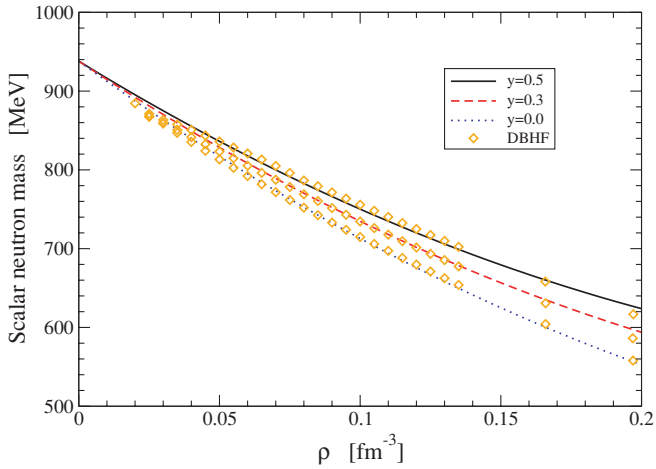


FIG. 3. (Color online) Comparison between the best RMF adjustment and the scalar mass calculated with the DBHF approach. The asymmetry parameter $y = \rho_p/\rho_B$ ranges from 0.5 to 0. It clearly shows a linear ($f_\sigma^2\rho_B$) and a quadratic ($f_\sigma^{\rm nl}\rho_B^2$) behavior in the baryonic density. The isospin asymmetry is also well reproduced by the linear term $f_\delta^2\rho_3$ in the asymmetry density $\rho_3$.

### B. Determination of the $\omega$ and $\rho$ coupling constants

In contrast to DBHF theory, which shows a nonlinear convergence to zero in the binding energy, RMF theory converges smoothly. We show in Fig. 4 (top panel) a comparison between the DBHF calculation and the low-density functional RMF for the density of energy, $E/V$, and the binding energy, $E/A$. Recall that the nonlinear term $\epsilon_{\rm NL,9}$ defined in Eq. (16) has to be divided by 2. The low-density effects are reduced on the energy density plot compared to the effects on the binding energy. In fact, as $E/V = \rho_B E/A$, the low-density behavior of the binding energy is strongly reduced by the factor of $\rho_B$ in the

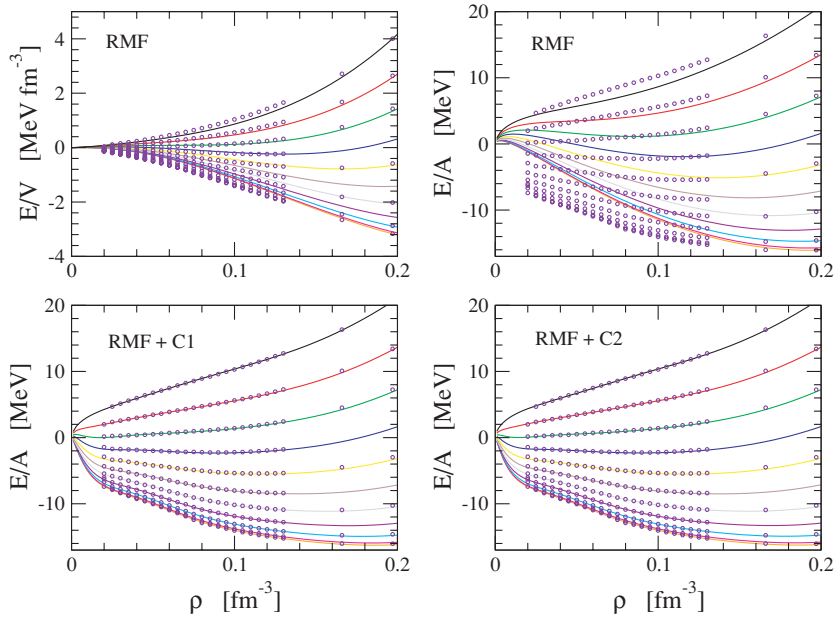


FIG. 4. (Color online) Comparison of the DBHF results (circle points) and the low-density functionals in asymmetric nuclear matter. On the top panels are shown the energy density and the binding energy for the parameters RMF; on the bottom panels are shown the binding energies for the corrected functionals RMF+C1 and RMF+C2.

energy density. Therefore, we adjust the mean-field functional on the energy density obtained from the DBHF calculation in asymmetric nuclear matter, where the low-density effects are weaker. We also force the functional to reproduce exactly the DBHF calculations at $\rho_B = 0.197$ fm$^{-3}$ in symmetric nuclear matter and pure neutron matter. This constraint ensures that the symmetry energy at saturation density is well reproduced. Table I resumes the parameters obtained from the low-density functional RMF. In the following section, we propose a correction of the functional to take into account the correlations beyond the mean field.

### C. Corrections to the mean-field functional RMF

As already discussed and shown in Figs. 1 and 4, ab initio calculations such as relativistic or nonrelativistic Brueckner calculations have a completely different low-density behavior compared to standard mean-field prediction. For neutron matter this is a known fact and has also been investigated in the—hypothetical—unitary limit $ak_F \to \infty$, where $a$ is the $nn$ scattering length. In this limit many-body calculations (BHF, variational, and GFMC) lead to a different low-density behavior than RMF theory (see the discussion in Ref. [27]). To account for the low-density behavior of the DBHF EOS one has therefore to go beyond the standard prediction of mean-field theory.

In this paper we choose a pragmatic approach and propose a fit of the difference between the DBHF EOSe and the low-density RMF functional. Thus we add two new functions $g^S(\rho_B)$ and $g^N(\rho_B)$ to the energy density so that

$$\epsilon_{\mathrm{DBHF}}(\rho_n, \rho_p) = \epsilon_{\mathrm{RMF}}(\rho_n, \rho_p) + (1-\beta^2)g^S(\rho_B) + \beta^2 g^N(\rho_B), \quad (18)$$

where $\beta = (\rho_n - \rho_p)/\rho_B$. The additional terms $g^S(\rho_B)$ and $g^N(\rho_B)$ are, respectively, adjusted in symmetric nuclear matter and pure neutron matter. The isospin degree of freedom is factorized with a quadratic function that respects the nuclear isospin symmetry. This approximation is often performed (see, e.g., Ref. for [1]), but in our case, it is also justified afterward by comparing the new functionals RMF+C1 and RMF+C2 to the DBHF binding energies at low densities (Fig. 4, bottom panels). The functional correction is unknown, but it is clear that this correction should be small around saturation density and should converge to zero at very small densities. Then an overall exponential shape imposed to fulfill the first condition and a factorization in power of the density ensure that the second condition is also satisfied. We obtained two different density functionals that reproduce the data with equal accuracy. The first phenomenological correction C1 is a product of a polynomial function in the baryonic density with an exponential and has the following form:

$$g^S(\rho_B) = \frac{\rho_B}{0.06}\left(v_0^S + v_1^S\rho_B + v_2^S\rho_B^2\right)e^{-(\rho_B/\rho_0^S)^{1.2}}, \quad (19)$$

$$g^N(\rho_B) = \left(\frac{\rho_B}{0.1}\right)^2 v_0^N e^{-(\rho_B/\rho_0^N)^2}, \quad (20)$$

TABLE I. The parameters of the functional reproducing the scalar mass and the energy density of the DBHF calculation compared to the parameters proposed in Ref. [42].

| Fits | $f_\sigma$ (MeV$^{-1}$) | $f_\sigma^{\mathrm{nl}}$ (MeV$^{-2}$ fm$^3$) | $f_\delta$ (MeV$^{-1}$) | $f_\omega$ (MeV$^{-1}$) | $f_\rho$ (MeV$^{-1}$) |
|---|---|---|---|---|---|
| RMF | $1.693 \times 10^{-2}$ | $3.735 \times 10^{-4}$ | $7.242 \times 10^{-3}$ | $1.299 \times 10^{-2}$ | $8.843 \times 10^{-3}$ |
| set A NL$\rho\delta$ [42] | $1.629 \times 10^{-2}$ | $9.35 \times 10^{-4}$ | $8.013 \times 10^{-3}$ | $1.18 \times 10^{-2}$ | $8.996 \times 10^{-3}$ |

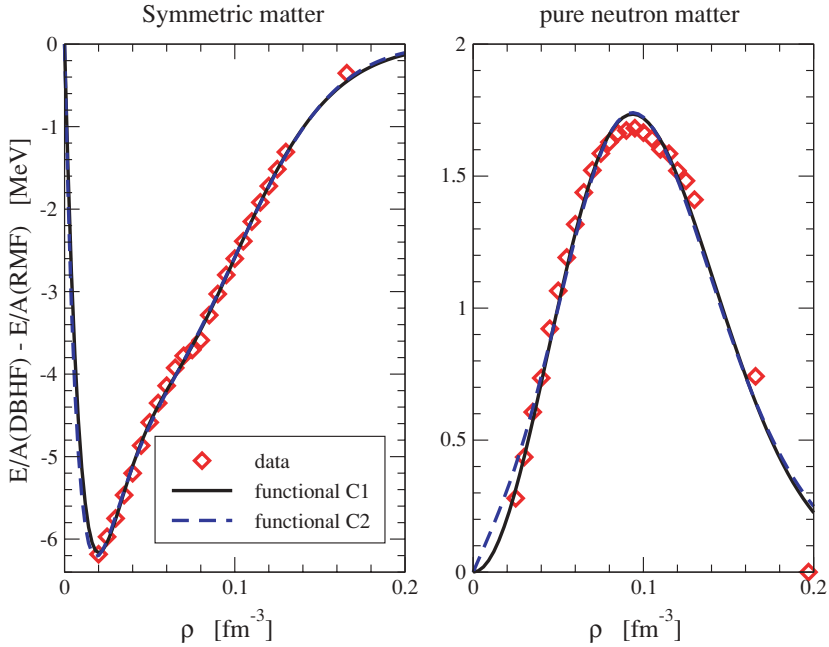


FIG. 5. (Color online) Difference between the DBHF calculation and the low-density RMF fit (square symbols). The corrections (solid lines) are drawn for symmetric nuclear matter (left panel) and pure neutron matter (right panel).

with the parameters: $v_0^S = -48.834$ MeV fm$^3$, $v_1^S = 1073.3$ MeV fm$^6$, $v_2^S = -14813$ MeV fm$^9$, $\rho_0^S = 0.03114$ fm$^{-3}$, $v_0^N = 5.373$ MeV fm$^6$, and $\rho_0^N = 0.0937$ fm$^{-3}$. The second phenomenological correction C2 is a sum of two exponentials of the form

$$g^S(\rho_B) = v_0^S \frac{\rho_B}{0.01} e^{-\rho_B/\rho_0^S} + v_1^S \frac{\rho_B}{0.06} e^{-(\rho_B/\rho_1^S)^2}, \quad (21)$$

$$g^N(\rho_B) = v_0^N \frac{\rho_B}{0.01} e^{-(\rho_B/\rho_0^N)^{2.2}} + v_1^N \frac{\rho_B}{0.1} e^{-(\rho_B/\rho_1^N)^2}, \quad (22)$$

with the parameters $v_0^S = -9.28$ MeV fm$^3$, $v_1^S = -5.48$ MeV fm$^3$, $\rho_0^S = 0.0140$ fm$^{-3}$, $\rho_1^S = 0.0879$ fm$^{-3}$, $v_0^N = -0.334$ MeV fm$^3$, $v_1^N = 4.818$ MeV fm$^3$, $\rho_0^N = 0.0629$ fm$^{-3}$, and $\rho_1^N = 0.1046$ fm$^{-3}$. We expect to have a measure of the error induced by the peculiar choice of the functional by comparing the prediction obtained with the two functionals RMF+C1 and RMF+C2.

In Fig. 5, we shown the result of the adjustment of the functional C1 (solid line) and C2 (dashed line) to the difference between the DBHF binding energy and the low-density RMF functional (square symbols) in symmetric nuclear matter (left panel) and pure neutron matter (right matter). Despite the different density dependence between the functionals C1 and C2, those two functionals reproduce the square symbols at the same level of accuracy.

### D. Properties of the functionals

Table II gives the properties of the functionals RMF, RMF+C1, and RMF+C2 around saturation density: the binding energy $B_0$, the saturation density $\rho_0$, the incompressibility $K_0$, and the symmetry energies $a_s^1$ and $a_s^2$. The properties of the DBHF calculation are also indicated. The properties of the low-density RMF functional differ significantly from the DBHF results. Indeed, the saturation density and the compression modulus are higher than the DBHF results. This is a consequence of the low value of the parameters $f_\sigma^{\rm nl}$, as expected. This parameter could not be changed, as it is already adjusted to the quadratic density dependence of the scalar mass. However, the saturation properties of the corrected functionals RMF+C1 and RMF+C2 are very close to the DBHF calculation. Then, in our framework, the reduction of the incompressibility modulus is induced by the low-density physics. This is a very different understanding from the standard one, which relies on nonlinear corrections at high densities. We have also calculated the symmetry energy in two different ways: either by assuming a quadratic dependence in the asymmetry parameter $\beta$ ($a_s^1$), or, because we have a functional, by performing the second derivative around symmetric nuclear matter ($a_s^2$). The latter calculation is the exact one. We note a systematic underestimation by about 1–2 MeV of the symmetry energy, assuming a quadratic behavior. This is a small error with respect to the difference in energy between symmetric nuclear matter and pure neutron matter.

In this context it is worth mentioning that RMF fits to finite nuclei require relatively high compression moduli $K \sim 300$ MeV [32,37]. Equations of state with a stiff high-

TABLE II. Properties of the functionals. The symmetry energy has been obtained in two different ways: assuming a quadratic dependence of the EOS between symmetric and pure neutron matter ($a_s^1$) or performing numerical derivation of the binding energy around symmetric nuclear matter ($a_s^2$). A systematic difference is observed but is less than 5%.

| Fits | $B_0$ (MeV) | $\rho_0$ (fm$^{-3}$) | $K_0$ (MeV) | $a_s^1$ (MeV) | $a_s^2$ (MeV) |
|---|---|---|---|---|---|
| RMF | −16.08 | 0.1933 | 365 | 35.8 | 37.7 |
| RMF+C1 | −16.27 | 0.1857 | 251 | 35.1 | 36.9 |
| RMF+C2 | −16.24 | 0.1856 | 242 | 35.1 | 36.9 |
| DBHF | −16.15 | 0.1814 | 230 | 34.4 | – |

density behavior stand, however, in contrast to the information extracted from heavy-ion reactions [46,47]. The pure RMF fits to the DBHF EOS (i.e., discarding the low-density correction term) provide equations of state that are stiff, however, not because of their high-density behavior but because of the low-density part. The compression moduli of the pure RMF contributions without correction terms are $K = 365$ MeV in contrast to the soft DBHF EOS with $K = 230$ MeV. If one assumes that the correction terms contain effectively contributions from the deuteron and/or reflect the precursor of a superfluid low-density state, which leads to additional binding in infinite matter but plays no substantial role in finite nuclei, this could explain the discrepancy between the EOS obtained from RMF fits to finite nuclei and that predicted by DBHF or the a low-density virial expansion [7].

## V. SPINODAL INSTABILITIES

Let us consider asymmetric nuclear matter characterized by proton and neutron densities $\rho_i = \rho_p, \rho_n$. In infinite matter, the extensibility of the free energy implies that it can be reduced to a free energy density: $F(T, V, N_i) = V\mathcal{F}(T, \rho_i)$. The system is stable against separation into two phases if the free energy of a single phase is lower than the free energy in all two-phase configurations. This stability criterion implies that the free energy density is a convex function of the densities $\rho_i$. A local necessary condition is the positivity of the curvature matrix:

$$[\mathcal{F}_{ij}] = \left[\left.\frac{\partial^2 \mathcal{F}}{\partial\rho_i \partial\rho_j}\right|_T\right] \equiv \left[\left.\frac{\partial \mu_i}{\partial\rho_j}\right|_T\right], \tag{23}$$

where we have introduced the chemical potentials $\mu_j \equiv \frac{\partial F}{\partial N_j}|_{T,V,N_i} = \frac{\partial \mathcal{F}}{\partial \rho_j}|_{T,\rho_{i\neq j}}$. In the considered two-fluid system, the $[\mathcal{F}_{ij}]$ is a $2 \times 2$ symmetric matrix, so it has two real eigenvalues,

$$\lambda^{\pm} = \frac{1}{2}\left(\mathrm{Tr}[\mathcal{F}_{ij}] \pm \sqrt{\mathrm{Tr}[\mathcal{F}_{ij}]^2 - 4\mathrm{Det}[\mathcal{F}_{ij}]}\right), \tag{24}$$

associated with eigenvectors $\delta\rho^{\pm}$ defined by $(i \neq j)$

$$\frac{\delta\rho_j^{\pm}}{\delta\rho_i^{\pm}} = \frac{\mathcal{F}_{ij}}{\lambda^{\pm} - \mathcal{F}_{jj}} = \frac{\lambda^{\pm} - \mathcal{F}_{ii}}{\mathcal{F}_{ij}}. \tag{25}$$

The sign of the eigenvalue indicates the direction of the instability. It defines a local order parameter since it is the direction along which the phase separation occurs. The eigenvalues $\lambda$ define sound velocities, $c$, by $c^2 = \frac{1}{18m}\rho_1\lambda$. In the spinodal area, the eigenvalue $\lambda$ is negative, so the sound velocity is purely imaginary and the instability time $\tau$ is given by $\tau = d/|c|$, where $d$ is a typical size of the density fluctuation.

The requirement that the local curvature is positive is equivalent to the requirement that both the trace $(\mathrm{Tr}[\mathcal{F}_{ij}] = \lambda^+ + \lambda^-)$ and the determinant $(\mathrm{Det}[\mathcal{F}_{ij}] = \lambda^+\lambda^-)$ are positive, that is,

$$\mathrm{Tr}[\mathcal{F}_{ij}] \geqslant 0 \quad \text{and} \quad \mathrm{Det}[\mathcal{F}_{ij}] \geqslant 0. \tag{26}$$

The use of the trace and the determinant, which are two basis-independent characteristics of the curvature matrix, clearly stresses the fact that the stability analysis should be independent of the arbitrary choice of the thermodynamical quantities used to label the state [e.g., $(\rho_p, \rho_n)$ or $(\rho_1, \rho_3)$]. If Eq. (26) is violated the system is in the unstable region of a phase transition.

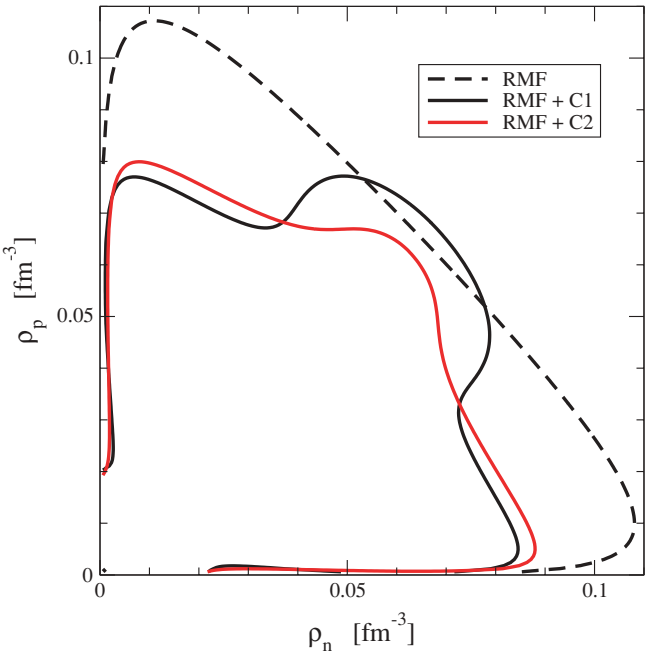


FIG. 6. (Color online) Spinodal contour for the low-density RMF functional, RMF, RMF+C1, and RMF+C2.

We represent in Fig. 6 the spinodal contour for the low-density RMF functional, RMF, RMF+C1, and RMF+C2. The contour for the RMF functional is very similar to the one obtained previously with nonrelativistic interactions [6,48,49]. Meanwhile, spinodal densities are a little bit larger. Indeed, in mean-field models, it is well known that the spinodal density in symmetric nuclear matter scales with the saturation density [50]. The spinodal densities we obtain is just due to a scaling effect induced by the saturation density, which is slightly to large for the functional RMF. The corrections induce important modifications of the spinodal contour, especially in asymmetric nuclear matter. For an asymmetry parameter of about $y \sim 0.4$, the spinodal density $\rho_s$ is reduced by about 15–20%.

In usual mean-field calculations, it has been found that the direction of the unstable mode is still isoscalar in asymmetric nuclear matter [6]. Because the spinodal contour calculated with the functionals RMF+C1 and RMF+C2 differs significantly from the functional RMF, one could wonder what would be the consequences for the unstable mode: Would it still be isoscalar or possibly isovector? We have represented our results on Fig. 7, which shows the evolution of the unstable mode $\delta\rho_n/\delta\rho_p$ with density for asymmetries ranging from $y = 0.1$ to 0.5. We represent only neutron-rich matter; the curves for proton-rich matter are easily deduced from the isospin symmetry property. An isoscalar mode is defined by $\delta\rho_n/\delta\rho_p = 1$ whereas a mode along $y =$ constant satisfies $\delta\rho_n/\delta\rho_p = y/(1-y)$. For the convenience of understanding

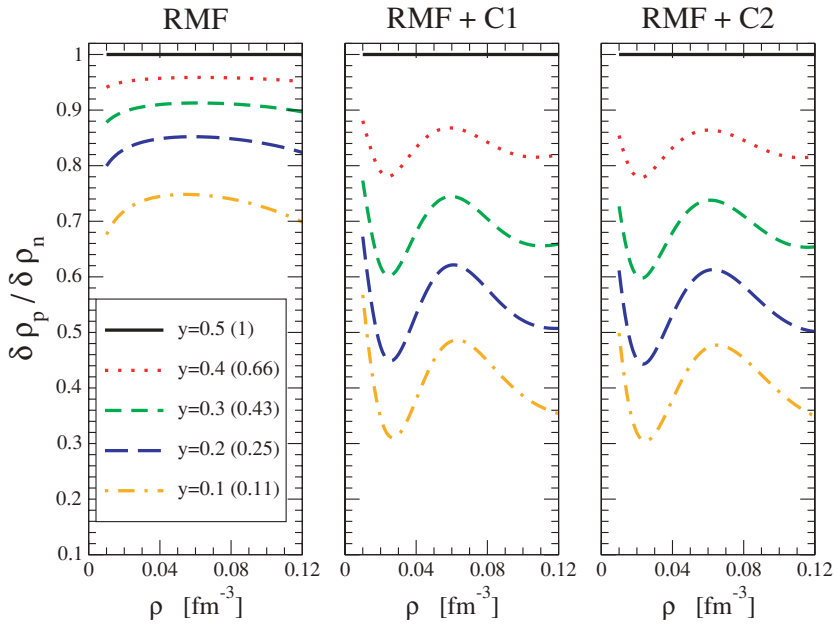


FIG. 7. (Color online) Evolution of the unstable mode $\delta\rho_n/\delta\rho_p$ with the density for asymmetries ranging from $y = 0.1$ to 0.5.

Fig. 7, the value $y/(1-y)$ is written in parentheses in the legend of each curve. For the three functionals (RMF, RMF+C1, and RMF+C2) the unstable mode is included in between the isoscalar direction and the direction $y =$ constant. However, the results obtained with the functionals RMF+C1 and RMF+C2 are very similar and differ from the one obtained with the functional RMF. Indeed, for the functionals RMF+C1 and RMF+C2, the unstable mode is less isoscalar than the one calculated with the functional RMF; hence, the fractionation mechanism should be less pronounced than the one predicted with mean-field models [6,48,49]. The gas phase should then be less asymmetric than what was previously predicted based on mean-field calculations.

## VI. CONCLUSIONS

We have obtained two functionals taht give a very good description of the DBHF calculations in asymmetric nuclear matter. Those functionals are based on the low-density RMF Lagrangian, which is developed as a series expansion of $k_F/M$. Effective terms are added to account for effects beyond the mean field such as the deuteron pole. This parametrization has been used to understand the topological properties of the energy density, such as the spinodal zone. We have observed that the spinodal zone is reduced in asymmetric nuclear matter, in contrast to all the previous mean-field calculations. Based on the analysis of the direction of the unstable mode, it is shown that the gas phase could be less asymmetric than what was previously predicted based on mean-field calculations.

This calculation has been performed at zero temperature whereas experiments probe the liquid-gas phase transition near the critical temperature [50]. An extension of this work to finite temperature is then necessary, but one could expect from mean-field calculations that the critical density scales with the spinodal density $\sim 0.5\rho_s$. In a future work, it would then be interesting to evaluate the effects of the two-body correlations at finite temperature.

As a final conclusion and outlook of this work, we would like to stress that the low-density EOS is required for both heavy-ion collisions as well as for the description of the crust of neutron stars where a low-density neutron gas is formed. The density functional theory is then an interesting framework where these two different nuclear systems could be described by a unique functional.

## ACKNOWLEDGMENTS

This work has been supported by the Deutsche Forschungsgemeinschaft (DFG) under Contract No. FA 67/29–1 and by the Spanish Ministry of Education and Science under Grant No. SB-2005–0131.

## APPENDIX A: RELATIVISTIC MEAN-FIELD MODEL

A set of coupled field equations for the meson and nucleon fields can be obtained from the Lagrangian in Eq. (1). The field equations in a mean-field approximation (MFA) are

$$[i\gamma_\mu\partial^\mu - (M - g_\sigma\sigma - g_\delta\tau_3\delta_3) - g_\omega\gamma^0\omega_0 - g_\rho\gamma^0\tau_3\rho_0]\psi = 0, \tag{A1}$$

$$m_\sigma^2\sigma + a\sigma^2 + b\sigma^3 = g_\sigma\langle\bar\psi\psi\rangle = g_\sigma\rho_s, \tag{A2}$$

$$m_\omega^2\omega_0 = g_\omega\langle\bar\psi\gamma^0\psi\rangle = g_\omega\rho_B, \tag{A3}$$

$$m_\rho^2\rho_0 = g_\rho\langle\bar\psi\gamma^0\tau_3\psi\rangle = g_\rho\rho_3, \tag{A4}$$

$$m_\delta^2\delta_3 = g_\delta\langle\bar\psi\tau_3\psi\rangle = g_\delta\rho_{s3}, \tag{A5}$$

where $\rho_3 = \rho_p - \rho_n$ and $\rho_{s3} = \rho_{sp} - \rho_{sn}$, and where $\rho_B = \rho_p + \rho_n$ and

$$\rho_{si} = \frac{\gamma}{(2\pi)^3}\int_0^{k_{F_i}} d^3k\,\frac{M_i^*}{E_i^*(k)} \tag{A6}$$

are the baryon and the scalar densities, respectively.

By neglecting the derivatives of mesons fields, the energy-momentum tensor in the MFA can be given by

$$T_{\mu\nu} = i\bar{\psi}\gamma_\mu\partial_\nu\psi + \left[\tfrac{1}{2}m_\sigma^2\sigma^2 + U(\sigma) + \tfrac{1}{2}m_\delta^2\vec{\delta}^2 - \tfrac{1}{2}m_\omega^2\omega_\lambda\omega^\lambda - \tfrac{1}{2}m_\rho^2\vec{\rho}_\lambda\vec{\rho}^\lambda\right]g_{\mu\nu}. \quad \text{(A7)}$$

The equation of state (EOS) for nuclear matter at $T = 0$ is straightforwardly obtained from the energy-momentum tensor. The energy density has the form

$$\epsilon = \langle T^{00}\rangle = \sum_{i=n,p} 2\int \frac{\mathrm{d}^3k}{(2\pi)^3}E_i^*(k) + \frac{1}{2}m_\sigma^2\sigma^2 + U(\sigma) + \frac{1}{2}m_\omega^2\omega_0^2 + \frac{1}{2}m_\rho^2\rho_0^2, + \frac{1}{2}m_\delta^2\delta_3^2. \quad \text{(A8)}$$

The pressure is given by

$$p = \frac{1}{3}\sum_{i=1}\langle T^{ii}\rangle = \sum_{i=n,p}\frac{2}{3}\int\frac{\mathrm{d}^3k}{(2\pi)^3}\frac{k^2}{E_i^*(k)} - \frac{1}{2}m_\sigma^2\sigma^2 - U(\sigma) + \frac{1}{2}m_\omega^2\omega_0^2 + \frac{1}{2}m_\rho^2\rho_0^2 - \frac{1}{2}m_\delta^2\delta_3^2, \quad \text{(A9)}$$

where $E_i^*(k) = \sqrt{k^2 + {M_i}^{*2}}$, $i = p, n$. The nucleon Dirac masses are, respectively,

$${M_p}^* = M - g_\sigma\sigma - g_\delta\delta_3, \quad \text{(A10)}$$

$${M_n}^* = M - g_\sigma\sigma + g_\delta\delta_3. \quad \text{(A11)}$$

In the MFA the kinetic contributions to the energy density and pressure in Eqs. (A8) and (A9) can easily be evaluated by partial integration, which yields

$$\epsilon_{\mathrm{kin}} = \sum_{i=n,p} 2\int\frac{\mathrm{d}^3k}{(2\pi)^3}E_i^*(k) = \sum_{i=n,p}\left(\frac{3}{4}\rho_i E_i^*(k_{F_i}) + \frac{1}{4}M_i^*\rho_{si}\right), \quad \text{(A12)}$$

$$p_{\mathrm{kin}} = \sum_{i=n,p}\frac{2}{3}\int\frac{\mathrm{d}^3k}{(2\pi)^3}\frac{k^2}{E_i^*(k)} = \sum_{i=n,p}\left(\frac{1}{4}\rho_i E_i^*\left(k_{F_i}\right) - \frac{1}{4}M_i^*\rho_{si}\right). \quad \text{(A13)}$$

The nucleon chemical potentials $\mu_i$ are given in terms of the vector meson mean fields:

$$\mu_i = \sqrt{k_{F_i}^2 + {M_i}^{*2}} + g_\omega\omega_0 \mp g_\rho\rho_0(+\text{proton}, -\text{neutron}), \quad \text{(A14)}$$

where the proton and neutron Fermi momenta $k_{F_i}$ are related to the corresponding densities by $k_{F_i} = (3\pi^2\rho_i)^{1/3}$.

## APPENDIX B: SOLUTION METHOD OF THE NONLINEAR SELF-CONSISTENT EQUATION FOR THE ISOSCALAR SCALAR FIELD $\sigma$

Our starting point is the self-consistent equation (2). Let us call $\sigma_0$ the solution of this linear self-consistent equation, $g_\sigma\sigma_0 = f_\sigma^2\rho_s$, and $\sigma_1$ the first-order correction induced by the nonlinear terms. Then $\sigma_1$ fulfills the following equation:

$$g_\sigma\sigma_1 = -\frac{a}{g_\sigma m_\sigma^2}(g_\sigma\sigma_0 + g_\sigma\sigma_1)^2 - \frac{b}{(m_\sigma g_\sigma)^2}(g_\sigma\sigma_0 + g_\sigma\sigma_1)^3. \quad \text{(B1)}$$

We first suppose that $\sigma_1/\sigma_0 \ll 1$ (a hypothesis we will verify afterward). Then, Eq. (B1) leads to

$$\frac{\sigma_1}{\sigma_0} = -\frac{a}{m_\sigma^2}g_\sigma\sigma_0\left(1 + 2\frac{\sigma_0}{\sigma_1}\right) - \frac{b}{g_\sigma m_\sigma^2}(g_\sigma\sigma_0)^2\left(1 + 3\frac{\sigma_0}{\sigma_1}\right) + o\left(\frac{{\sigma_1}^2}{\sigma_0}\right). \quad \text{(B2)}$$

Indeed, it reads $2a\frac{\hbar}{m_\sigma}x + \frac{3b}{g_\sigma}x^2$, where $x = g_\sigma\sigma_0/m_\sigma = g_\sigma^2(\frac{\hbar}{m_\sigma})^3\rho_s$. With typical values, for example, from the NL3 model (i.e., $g_\sigma \sim 10, m_\sigma \sim 500$ MeV), the parameter $x$ is approximately $x = 1.6$ at saturation density. Then, the two terms in the denominator are about 20. The correction $\sigma_1/\sigma_0$ can be expressed as a function of the scalar density as

$$\frac{\sigma_1}{\sigma_0} = \frac{-\frac{ag_\sigma^2}{m_\sigma^4}\rho_s - \frac{bg_\sigma^3}{m_\sigma^6}\rho_s^2}{1 + 2\frac{ag_\sigma^2}{m_\sigma^4}\rho_s + 3\frac{bg_\sigma^3}{m_\sigma^6}\rho_s^2} + o\left(\frac{{\sigma_1}^2}{\sigma_0}\right) \quad \text{(B3)}$$

and taking into account only first-order corrections, we arrive at

$$g_\sigma\sigma_1 = -\frac{a}{g_\sigma m_\sigma^2}(g_\sigma\sigma_0)^2 + \left(\frac{2a^2}{g_\sigma^2 m_\sigma^4} - \frac{b}{(m_\sigma g_\sigma)^2}\right)(g_\sigma\sigma_0)^3 + o\left(g_\sigma\sigma_1^2\right). \quad \text{(B4)}$$

We keep only the first term, which contributes up to the power 9 in $k_{Fi}$. Hence, the approximate solution of the nonlinear self-consistent equation is

$$g_\sigma\sigma = f_\sigma^2\rho_s - \frac{af_\sigma^4}{g_\sigma m_\sigma^2}\rho_s^2 + o\left(k_{Fi}^9\right). \quad \text{(B5)}$$

The first term on the right-hand side of Eq. (B5) is the solution of the linear self-consistent equation; the second term is induced by nonlinear corrections.


[1] M. Baldo, C. Maieron, P. Schuck, and X. Viñas, Nucl. Phys. **A736**, 241 (2004).
[2] A. Sedrakian, Prog. Part. Nucl. Phys. **58**, 168 (2007).
[3] A. Sedrakian, T. T. S. Kuo, H. Müther, and P. Schuck, Phys. Lett. **B576**, 68 (2003).
[4] P. Gögelein and H. Müther, Phys. Rev. C **76**, 024312 (2007).
[5] B. A. Brown, Phys. Rev. Lett. **85**, 5296 (2000).
[6] V. Baran and J. Margueron, Eur. Phys. J. A **30**, 141 (2006); J. Margueron and Ph. Chomaz, Phys. Rev. C **71**, 024318 (2005); V. Baran, M. Colonna, M. DiToro, and V. Greco, Phys. Rev. Lett. **86**, 4492 (2001).
[7] C. J. Horowitz and A. Schwenk, Nucl. Phys. **A776**, 55 (2006).
[8] P.-G. Reinhard and M. Bender, Lect. Notes Phys. **641**, 249 (2004).

[9] M. Farine *et al*., J. Phys. G **25**, 863 (1999).
[10] P. Ring, Prog. Part. Nucl. Phys. **73**, 193 (1996); Lect. Notes Phys. **641**, 175 (2004).
[11] B. D. Serot and J. D. Walecka, Int. J. Mod. Phys. E **6**, 515 (1997).
[12] R. J. Furnstahl, Lect. Notes Phys. **641**, 1 (2004).
[13] M. Lutz, B. Friman, and Ch. Appel, Phys. Lett. **B474**, 7 (2000).
[14] P. Finelli, N. Kaiser, D. Vretenar, and W. Weise, Eur. Phys. J. A **17**, 573 (2003); Nucl. Phys. **A735**, 449 (2004).
[15] V. R. Pandharipande and R. B. Wiringa, Rev. Mod. Phys. **51**, 821 (1979).
[16] A. Akmal, V. R. Pandharipande, and D. G. Ravenhall, Phys. Rev. C **58**, 1804 (1998).
[17] M. Jaminon and C. Mahaux, Phys. Rev. C **40**, 354 (1989).
[18] W. Zuo, A. Lejeune, U. Lombardo, and J. F. Mathiot, Nucl. Phys. **A706**, 418 (2002).
[19] X. R. Zhou, G. F. Burgio, U. Lombardo, H.-J. Schulze, and W. Zuo, Phys. Rev. C **69**, 018801 (2004).
[20] M. Baldo and C. Maieron, J. Phys. G **34**, R243 (2007).
[21] B. ter Haar and R. Malfliet, Phys. Rep. **149**, 207 (1987).
[22] R. Brockmann and R. Machleidt, Phys. Rev. C **42**, 1965 (1990).
[23] F. de Jong and H. Lenske, Phys. Rev. C **58**, 890 (1998).
[24] T. Gross-Boelting, C. Fuchs, and A. Faessler, Nucl. Phys. **A648**, 105 (1999).
[25] C. Fuchs, Lect. Notes Phys. **641**, 119 (2004).
[26] E. N. E. van Dalen, C. Fuchs, and A. Faessler, Nucl. Phys. **A744**, 227 (2004).
[27] J. Carlson, J. Morales, V. R. Pandharipande, and D. G. Ravenhall, Phys. Rev. C **68**, 025802 (2003).
[28] W. H. Dickhoff and C. Barbieri, Prog. Part. Nucl. Phys. **52**, 377 (2004).
[29] A. Fabrocini, S. Fantoni, A. Y. Illarionov, and K. E. Schmidt, Phys. Rev. Lett. **95**, 192501 (2005).
[30] R. Machleidt, K. Holinde, and Ch. Elster, Phys. Rep. **149**, 1 (1987).
[31] B. D. Serot and J. D. Walecka, in *Advances in Nuclear Physics*, Vol. 16, edited by J. W. Negele and E. Vogt (Plenum, New York, 1986), p. 1.
[32] P. Ring, Prog. Part. Nucl. Phys. **73**, 193 (1996).
[33] O. Plohl, C. Fuchs, and E. N. E. van Dalen, Phys. Rev. C **73**, 014003 (2006); O. Plohl and C. Fuchs, Phys. Rev. C **74**, 034325 (2006).
[34] A. Tohsaki, H. Horiuchi, P. Schuck, and G. Röpke, Phys. Rev. Lett. **87**, 192501 (2001).
[35] M. Beyer, S. A. Sofianos, C. Kuhrts, G. Röpke, and P. Schuck, Phys. Lett. **B488**, 247 (2000).
[36] E. N. E. van Dalen, C. Fuchs, and A. Faessler, Phys. Rev. Lett. **95**, 022302 (2005); Phys. Rev. C **72**, 065803 (2005).
[37] G. A. Lalazissis, J. König, and P. Ring, Phys. Rev. C **55**, 540 (1997).
[38] S. Typel and H. H. Wolter, Nucl. Phys. **A656**, 331 (1999).
[39] C. Fuchs, H. Lenske, and H. H. Wolter, Phys. Rev. C **52**, 3043 (1995).
[40] S. K. Bogner, T. T. S. Kuo, and A. Schwenk, Phys. Rep. **386**, 1 (2003).
[41] B. D. Serot and J. D. Walecka, Int. J. Mod. Phys. E **6**, 515 (1997).
[42] B. Liu, H. Guo, M. Di Toro, and V. Greco, Eur. Phys. J. A **25**, 293 (2005).
[43] F. Hoffmann, C. M. Keil, and H. Lenske, Phys. Rev. C **64**, 034314 (2001); C. M. Keil, F. Hofmann, and H. Lenske, Phys. Rev. C **61**, 064309 (2000).
[44] T. Nikšić, D. Vretenar, and P. Ring, Phys. Rev. C **66**, 064302 (2002).
[45] S. S. Avancini, L. Brito, D. P. Menezes, and C. Providencia, Phys. Rev. C **70**, 015203 (2004).
[46] C. Sturm *et al*. (KaoS Collaboration), Phys. Rev. Lett. **86**, 39 (2001).
[47] C. Fuchs, A. Faessler, E. Zabrodin, and Y. M. Zheng, Phys. Rev. Lett. **86**, 1974 (2001); C. Fuchs, Prog. Part. Nucl. Phys. **56**, 1 (2006).
[48] C. Ducoin, Ph. Chomaz, and F. Gulminelli, Nucl. Phys. **A771**, 68 (2006).
[49] C. Ducoin, Ph. Chomaz, and F. Gulminelli, Nucl. Phys. **A781**, 407 (2007).
[50] Ph. Chomaz, M. Colonna, and Randrup, Phys. Rep. **389**, 263 (2004).